Aircraft Engineering and Aerospace Technology
2018, Volume 90, Issue 1, pp126-133

Large Eddy Simulation of Airfoil Self-Noise Using OpenFOAM

Abstract

Purpose – The purpose of this paper is to investigate airfoil self-noise generation and propagation by employing a hybrid method based on the Large-eddy simulation (LES) approach and Curle's acoustic analogy as implemented in OpenFOAM.

Design/methodology/approach – Large-eddy simulation of near-field flow over a NACA6512-63 airfoil at zero angle of attack with a boundary layer trip at *Re* = 1.9 × 10^5 has been carried out using the OpenFOAM® CFD code. Calculated flow results are compared with published experimental data. The LES includes the wind-tunnel installation effects by using appropriate inflow boundary conditions obtained from a RANS $k-\omega\ SST$ model computation of the whole wind tunnel domain. Far-field noise prediction was achieved by an integral method based on Curle's acoustic analogy. The predicted sound pressure levels are validated against the experimental data at various frequency ranges.

Findings – The numerical results presented in this paper show that the flow features around a NACA6512-63 airfoil have been correctly captured in OpenFOAM LES calculations. The mean surface pressure distributions and the local pressure peaks for the step-trip setup agree very well with the experimental measurements. Aeroacoustic prediction using Curle's analogy shows an overall agreement with the experimental data. The Sound Pressure Level (SPL)-frequency spectral analysis produces very similar data at low to medium frequency, whereas the experimentally observed levels are slightly overpredicted at a higher frequency range.

Practical implications – This study has achieved and evaluated an alternative aeroacoustic simulation method based on the combination of LES with a simple Smagorinsky SGS model and Curle's analogy, as implemented in the OpenFOAM CFD code. The unsteady velocity/pressure source data produced can be used for any simpler analytically-based far-field noise prediction scheme.

Originality/value – A complete integration of the LES and Curle's acoustic analogy for aeroacoustic simulations has been achieved in OpenFOAM. The capability and accuracy of the hybrid method are fully evaluated for high-camber airfoil self-noise predictions. Wind-tunnel installation effects have been incorporated properly into the LES.

Keywords Airfoil self-noise, OpenFOAM, Large Eddy Simulation, Curle's acoustic analogy

Paper type *Research paper*

Introduction

With the air traffic around the world rapidly increasing aircraft noise has become a widely recognised annoyance for the people living close to the airports. Therefore it has become a necessity to take effective measures to control aircraft noise for sustainable development in the aviation industry.

Aircraft noise reduction has progressed steadily in two directions, namely, aeroengine noise and airframe noise. The aeroengine noise has been reduced by a considerable level as explained by Li et al (2013). The increasingly stringent noise reduction targets established by the International Civil Aviation Organisation (ICAO) provide a lot of challenges on reducing airframe noise. Therefore extensive research is being carried out on all airframe noise problems. Among them, trailing edge noise, also called airfoil self-noise, is one of the key components in the total aircraft noise. Trailing edge noise is generated due to the scattering of turbulent eddies energy as developed in the boundary layer of the wings, high-lift devices and aeroengine fan blades, and is a key component of more complex airframe and high-lift device noise (flaps, slats and wing) and turbo-machinery noise (fan, turbine and compressor) in general. As many fundamental fan, turbine and compressor aeroacoustic problems have still not been fully explored and understood, the accurate prediction of noise generation by an isolated airfoil as obtained by careful computation of unsteady viscous flow around airfoil still remains an outstanding problem in experimental and computational aerodynamics.

One of the most popular and computationally efficient methods used for noise prediction is the integral method based on acoustic analogy, also referred to as a hybrid method. In this approach, the near-field flow obtained from a time-accurate solution model, such as URANS, DES and LES, are used to predict the far-field sound propagation with the aid of analytically derived integral solutions to wave equations. Compared to the direct method, in which both generation and propagation of sound waves are directly computed by solving the full Navier-Stokes equations, the integral method requires much less computational time, and therefore is a prime choice amongst engineers and scientists.

Large-eddy simulation (LES), which aims to solve numerically the larger turbulent scale fluctuations in space and time, while modelling the effect of more universal small turbulent scales using a subgrid-scale (SGS) model, is a promising approach for improving our understanding of trailing edge noise generation and providing data needed for the development of more practical engineering noise prediction methods.

In recent years, more and more companies and educational institutions have been shifting to an efficient open source CCM/CFD solver such as OpenFOAM to resolve their fluid dynamics problems due to its flexibility and accessibility, and avoid the higher cost of most commercial codes. The most popular and advanced turbulence simulation tools, such as LES and DES have been implemented in OpenFOAM. Curle's acoustic analogy has recently been implemented by Kraposhin and Strizhak (2013) to enable its application for aeroacoustic prediction, but this has not yet been widely applied and validated.

Thus, in the present study, OpenFOAM CFD code V2.1.0 has been employed to investigate the trailing edge noise generation and propagation around a high-cambered NACA6512-63 airfoil. First, unsteady Large-Eddy Simulation (LES) integrated with a Smagorinsky (1963) Sub-grid Scale (SGS) model are used to compute the near-field turbulence pressure and velocity field close to the airfoil trailing edge, and then the far-field sound pressure level is predicted from the source terms of the near-field flow using Curle's acoustic analogy. The computational results are validated against the experimental data of Winkler et al (2009) and their alternative numerical simulations carried out using the commercial code ANSYS® CFX V11 [Winkler et al. 2009, 2008, 2010].

The specific objectives of this study are: (1) to evaluate the capability and accuracy of the LES approach as implemented in OpenFOAM CFD code to capture the unsteady velocity and pressure field around the highly cambered NACA6512-63 airfoil, and the different boundary layer regimes associated with different noise generation mechanisms; (2) to access the capability and accuracy of the newly implemented Curle's acoustic analogy in OpenFOAM for aeroacoustic prediction; (3) to sample and analyse the surface pressure fluctuations to provide energy spectra in airfoil self-noise sources; (4) to produce accurate input data of an unsteady velocity/pressure source for developing any analytically-based far-field noise prediction scheme.

Methodology

In this section, the details of LES method and Curle's acoustic analogy are presented. The CFD model setting up and mesh details are discussed.

NACA6512-63 Airfoil and Mesh

The NACA6512-63 airfoil is an example of a highly cambered airfoil as typically used in highly loaded high-speed turbo-engine compressors. In the experimental setup considered by Winkler et al (2009), the NACA6512-63 airfoil was placed at 0° angle of attack with respect to the chord line. The airfoil had a chord length (c) of 13.5 cm and a span of 18 cm (≈1.33 c). The airfoil was placed in a flow that had a chord based Reynolds number of $R_{ec} = 1.9 \times 10^5$, which corresponds to a velocity of 21.11 m/s and Mach number of 0.062. The wind-tunnel nozzle exit was 18 × 18 cm^2 and the exit flow had a turbulence intensity of less than 0.2%. Three microphones were placed from 1.2 m and at different angles to the trailing edge (TE) to acquire the acoustic measurements (Winkler et al. 2009). Serration strips were added on both sides of the airfoil at around 10% of the chord to eliminate Tollmien-Schlichting (TS) instabilities and the extraneous noise that arise due to the large laminar flow region and the transition region in the vicinity of trailing edge. In order to represent the experimental setup accurately these trip devices were also incorporated into the simulations setup as a simplified

geometrical step-trip. From Winkler et al (2009) it was determined that such simplified step-trip configuration was sufficient enough to eliminate the tonal noise created due to the TS instabilities.

An airfoil with a small aspect ratio placed in a small dimension wind tunnel jet experiences a considerable deviation in the flow around it in comparison with an airfoil placed in a free-jet wind tunnel. From previous LES by Wang et al (2009), Addad et al (2008) and Moreau et al (2003) it was evident that the wind tunnel installation effects in such cases had to be taken into consideration in the present computations due to their evident influence.

Two computational domains were set up for numerical simulation, as shown in Figure 1. The complete wind tunnel domain (Figure 1 left) was used to model the wind tunnel installation effects on near-field flow around the airfoil. The wind tunnel domain has a size of 4.4 × 2.9 × 3.2 m and a total mesh size of 7 million structured hexa-cells. The truncated domain (Figure 2 right) was used for the high resolution LES around the NACA6512-63 airfoil. It was a very thin spanwise sector with a box size of 3.5 × 1 × 0.074c in the streamwise x, crosswise y and spanwise z directions, respectively. The multi-block structured C-H type mesh was generated with Salome V7.2.0 based on LES domain. The cell distribution along the airfoil was Lx × Ly × Lz = 896 × 100 × 32, and 200 grid points were distributed in wake region with denser node refinement close to the airfoil trailing edge. The grid resolution study by Winkler et al (2010) was used to determine the required span wise domain size and mesh resolution.

It is noted that one of the most significant issues with the LES is the grid-resolution requirements in the near-wall regions of flow. These areas can possess small streak-like structures requiring very fine mesh. In the present study, the radial C-grid lines away from the airfoil are clustered towards the airfoil surface boundary with normal spacing of the first grid away from the wall corresponding to $y^+ \approx 0.5 - 1$. In the spanwise direction, the grid spacing is uniformly distributed corresponding to $z^+ \approx 35$. The grid along streamwise direction corresponds to a spacing of $x^+ \approx 37$ and is clustered towards the airfoil leading edge (LE) and trailing edge (TE). The wake region of the domain was rotated by the wake deflection angle, as shown in Figure 1 right.

The simplified step-trip geometry, as shown in Figure 2, with a trip height of 80 μm and a trip length of 0.03c was used to replicate the boundary layer trip that was used in the experimental setup. The surface mesh over the airfoil in the region behind the trip was highly refined with around 170 gird points over a distance of 190 trip heights, in order to capture the expected boundary layer transition clearly.

The total mesh size for the whole LES domain was approximating 7 million cells.

Figure 1 Meshes for Wind-tunnel domain (left) and truncated LES Domain (right)

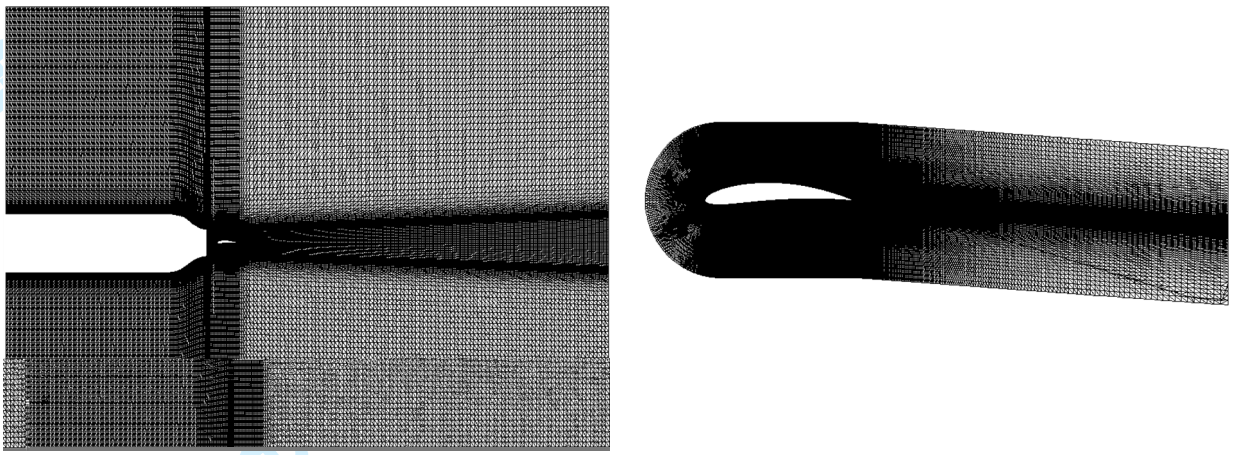

Figure 2 Refined meshes behind the simplified step-trip on the airfoil Surface

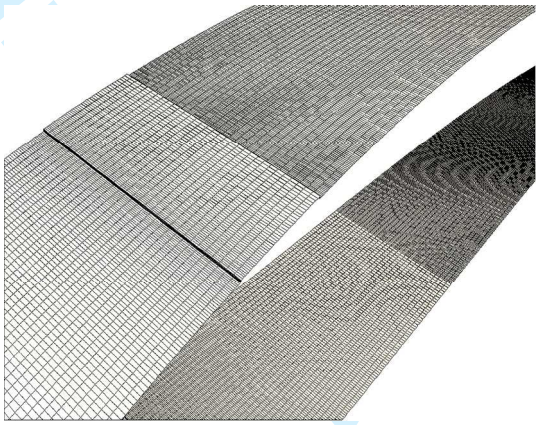

Numerical Method

In this study LES as implemented in OpenFOAM V2.0.1 was applied. A pressure Implicit with Splitting of Operator (PISO) algorithm was used to resolve the incompressible Navier-Strokes equations with Smagorinsky Sub-grid Scale (SGS) model (Smagorinsky, 1963) for the near-field flow around the airfoil. An initial steady-state simulation with Reynolds-averaged Navier–Stokes (RANS) equations was performed for the whole wind tunnel domain, in which the $\kappa - \omega$ Shear Stress Transport (SST) equations are used with a SIMPLE algorithm to provide the inflow boundary conditions for the 3D LES domain.

In the Smagorinsky model the eddy viscosity ν_{SGS} is obtained by assuming that the small scales are in equilibrium, so that energy production and dissipation are in balance. This yield,

$$\nu_{SGS} = 2\overline{\rho}(C_s\Delta)^2\left|\widetilde{S}\right| = 2\overline{\rho}(C_s\Delta)^2(2\widetilde{S}_{ij}\widetilde{S}_{ij})^{1/2} \quad (1)$$

Where C_s is the Smagorinsky constant, Δ equals the filter cutoff width, i.e. the characteristic length scale of the SGS eddies and $|\widetilde{S}|$ represents the absolute value of the shear strain tensor. Suggested value of the constant ranges between 0.065 – 0.25 (Ferzinger et al, 1996). For our specific case the constant $C_s = 0.17$ was used, which was derived from similar previous studies (Matouk et al, 2015, Gilling, 2009). Since this model can be excessively diffusive, especially near walls. One possible solution would be to diminish the value of C_s near walls, thus limiting the near wall eddy viscosity. Ferziger and Peric (1996) suggest that the eddy viscosity should be damped by using the model for van Driest damping function,

$$C_s = C_{s0}(1 - e^{-n+/A+})^2 \quad (2)$$

where n^+ is the normal distance from the viscous wall units and A^+ is a constant, usually taken as 25 (Vedovoto et al, 2015).

In OpenFOAM LES, the filtering between the larger turbulence scales that have to be directly resolved by N-S equations and the smaller scales modelled by SGS model was achieved using Eqn (3) and (4), in which Δ is the filter width and defined as the cube root of cell volume. Eqn (3) is written in a one dimensional velocity field. An over-bar denotes the large scales, whereas the small scales are denoted by the prime superscript.

$$\overline{u_i} = \oint u_i(x') G(x, x'; \Delta) dx' \quad (3)$$

where,

u_i	One dimensional velocity
Δ	Length scale threshold
$G(x, x'; \Delta)$	Filter kernel that should satisfy the following condition

$$\oint G(x, x'; \Delta) dx' = 1 \quad (4)$$

In OpenFOAM, the first filter level generally uses an implicit top-hat filter as a standard filter. In this case grid spacing and discretization schemes guide the filtering, where the grid spacing would be the filter width and the averaged local value of $\bar{u}_i$ will be equal. Eqn (5) gives the top-hat filtering function.

$$G(x,\Delta) = \begin{cases} \frac{1}{\Delta}, & if\,|x'| \le \frac{\Delta}{2} \\ 0, & otherwise \end{cases} \quad (5)$$

The time step for the unsteady LES was selected as $\Delta t = 5 \times 10\text{-}6s$ so that the Courant-Friedrichs-Lewy (CFL) number stays under 1. This corresponds to a sampling frequency of 100 kHz and it has proved sufficient enough for the current simulation. Turbulence samples were collected after the initial turbulent flow field had settled down. The running time to gather turbulence statistics corresponded to approximately 10 flow-through times based on freestream velocity and the airfoil chord length. The running time required was 2816 CPU hours per flow through time.

Curle's Acoustic Analogy

In this study, the Curle's acoustic analogy as newly implemented in OpenFOAM has been employed for far-field sound pressure level prediction. Based on Lighthill's general theory of aerodynamic sound (Lighthill, 1952), Curle provided an extension to Lighthill's analogy to incorporate the influence of the solid boundaries on noise generation (Curle, 1955). According to Curle's theory, two points should be added into the global sound generation:

- The sound generated from the quadrupoles of Lighthill's acoustic analogy will be calculated taking into consideration of the reflection and diffraction due to the presence of solid boundaries.
- Dipole sources are generated due to the interaction between the fluid and the solid boundary.

Full Details of the Curle's acoustic analogy and its implementation in OpenFOAM are given in Reference (Curle, 1955). Only some key equations and issues relevant to the present application are highlighted here.

In Lighthill's acoustic analogy, the inhomogeneous wave equation is:

$$\frac{\partial^2 \rho'}{\partial t^2} - c_0 \frac{\partial^2 \rho'}{\partial x^2{}_i} = \frac{\partial^2 T_{ij}}{\partial x_i \partial x_j} \quad (6)$$

Where Lighthill's stress tensor is defined in Eqn (7):

$$T_{ij} = \rho u_i u_j + \delta_{ij}(p' - c^2{}_0 \rho') - \tau_{ij} \quad (7)$$

Here, $\frac{\partial^2 \rho_0}{\partial t^2} = 0$, and

T_{ij} - Lighthill's stress tensor

c_0 - Speed of sound

δ_{ij} - Kronecker delta

Eqn (6) does not contain any assumption thus can be regarded as the exact equation containing the physics for the propagation. This equation can be viewed as an inhomogeneous wave equation with assumptions such that the right hand term of the equation is known independent of the left hand term, ensuring that sound propagation is separated from its source.

Curle's acoustic analogy extended Lighthill's analogy by including an additional term $\partial f_i/\partial x_i$ to the right had side of the Eqn (6). Compared to quadrupole sources, dipole sources are much more efficient noise mechanism at low Mach numbers. The radiated sound will be reflected and diffracted by the solid boundaries changing the wave characteristics. Finally the quadrupole sources can be neglected as only the dipole sources are often used for calculating the acoustic field.

The most general form of the Lighthill's inhomogeneous wave equation's solution is shown as:

$$\rho' = \frac{1}{4\pi c^2{}_0}\int_V \frac{\partial^2 T_{ij}}{\partial y_i y_j}\frac{1}{|x-y|}dV(y) + \frac{1}{4\pi}\int_S \left\{\frac{1}{r}\frac{\partial p}{\partial n} + \frac{1}{r^2}\frac{\partial r}{\partial n}\rho + \frac{1}{c_0 r}\frac{\partial r}{\partial n}\frac{\partial \rho}{\partial t}\right\}dS(y) \tag{8}$$

In Eqn (6), $\partial^2 T_{ij}/\partial y_i y_j$, $\partial\rho/\partial t$, and $\partial\rho/\partial n$ are calculated at lagging times $t - r/c_0$, where $r = |x-y|$.

x	Location of the sound source
y	Location of the observer
n	Outward normal of the fluid
V	Total volume external to solid boundaries
S	Surface of the solid boundaries

Curle simplified Eqn (8) by introducing the free-space Green's function and further simplifying it mathematically to Eqn (9):

$$\rho(x,t) = \frac{1}{4\pi c^2{}_0}\frac{\partial^2}{\partial x_i x_j}\int_V \frac{T_{ij}}{r}dV(V) - \frac{1}{4\pi c^2{}_0}\frac{\partial}{x_i}\int_S \frac{n_i}{r}\left(\rho\delta_{ij} - \tau_{ij}\right)dS(y) \tag{9}$$

The complete derivation can be referred to Goldstein (1976). The derivatives within the integrals are solved and $\rho' = p'/c^2{}_0$ are applied to achieve a far field approximation, as shown in Eqn (10):

$$p'(x,t) \cong \frac{x_i x_j}{4\pi\|x\|^2 c^2{}_0}\frac{\partial^2}{\partial t}\int_V \left[\frac{T_{ij}}{r}\right]_{te} dV(y) - \frac{1}{4\pi}\frac{\partial}{\partial t}\int_S \left[\frac{\rho\upsilon_i}{r}\right]_{te} n_i dS - \frac{x_j}{4\pi\|x\|c_0}\frac{\partial}{\partial t}\int_S \frac{P_{ij} + \rho\upsilon_i\upsilon_j}{r} n_i dS \tag{10}$$

The retarded time te over the surface can be neglected assuming that the source region acts as a compact body, and rewriting $r = |x|$ with $y = 0$ if it is at the origin inside the body. The surface velocities υ_i and υ_j are zero. The hydrodynamic pressure that is contained within the stress tensor $P_{ij} = p\delta_{ij} - \sigma_{ij}$ and the viscosity term σ_{ij} are not taken into consideration for further calculation. Therefore the simplified equation is:

$$p'(x,t) \cong \frac{x_i x_j}{4\pi \|x\|^3 c^2{}_0} \frac{\partial^2}{\partial} \int_V [T_{ij}] dV(y) - \frac{x_j}{4\pi \|x\|^2 c_0} \frac{\partial}{\partial t} \int_S p n_i dS \quad (11)$$

For flows at low Mach number the first integral in Eqn (11) can be neglected so as to ignore the quadrupole sources. Several other assumptions were made in order to formulate Eqn (11), more details are provided in reference (Curle, 1955).

Results and Discussions

In this section, the results from LES on noise sources in near-field flow and sound propagation in far field from acoustic analogy prediction are presented and analysed.

Flow Field Description

Figure 3 and 4 illustrates the main characteristics of the near-field flow around the NACA6512-63 airfoil. The streamlines of the instantaneous flow field around the trailing edge and downstream of the step-trip are shown in Figure 3(a) and (b), respectively. The presence of a fixed vortex just downstream of the step-trip on the airfoil pressure side is clearly observed in Figure 3(b), accompanying a small scale boundary layer separation. The boundary layer flow at the airfoil suction side experiences separation near the trailing edge at x/c = 0.8, after that strong turbulent flow appears causing larger velocity variation, as shown in Figure 3(a). The reattachment of the boundary layer on the suction side occurs at x/c = 0.95. Similar reattachment can be seen on the pressure surface around x/c = 0.45. The step-trip configuration does not show any obvious effect on boundary layer flow on the suction side, which indicates that the step-trip is not sufficient enough to disturb the boundary layer and cause turbulence transition in the accelerated flow.

A standard method used to identify turbulence coherent structures formed around airfoil is the Q-criterion visualization, where Q is the second invariant of the velocity-gradient tensor and is defined by,

$$Q = \frac{1}{2}\left(\Omega_{ij}\Omega_{ij} - S_{ij}S_{ij}\right) = \frac{1}{2}\frac{\nabla^2 p}{\rho} \quad (12)$$

Where the Ω_{ij} and S_{ij} are the anti-symmetric and symmetric part of the velocity gradient respectively, that is,

$$\Omega_{ij} \equiv \frac{1}{2}\left(\frac{\partial u_i}{\partial x_j} - \frac{\partial u_j}{\partial x_i}\right) \tag{13}$$

$$S_{ij} \equiv \frac{1}{2}\left(\frac{\partial u_i}{\partial x_j} + \frac{\partial u_j}{\partial x_i}\right) \tag{14}$$

Figure 3 Streamlines of instantaneous velocity around airfoil trailing edge (a) and step-trip on the pressure side (b)

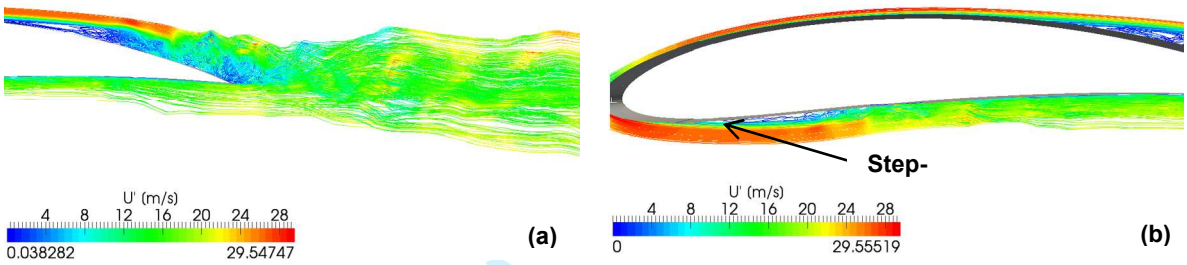

Figure 4 Iso-surfaces of Q-criterion on the airfoil suction side (left) and pressure side (right)

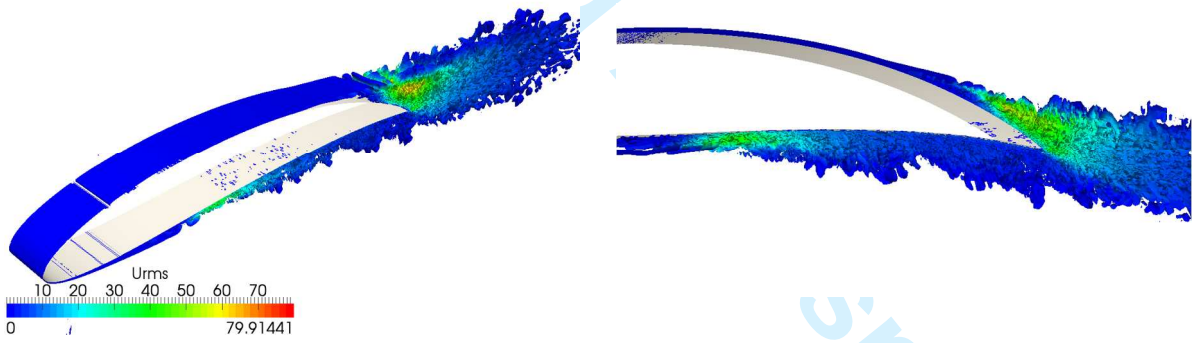

The Q-criterion thus represents the balance between the rate of vorticity $\Omega^2 = \Omega_{ij}\Omega_{ij}$ and the rate of strain $S^2 = S_{ij}S_{ij}$. In the core of a vortex, $Q > 0$, since vorticity increases as the center of the vortex is approached. Thus regions of positive Q-criterion correspond to vortical structures. This type of visualization allows the identification of rotational motion from non-rotational motions. An average iso-surface for Q-criterion of Q = 2 × $10^5 s^{-2}$ is used for visualization.

In Figure 4, the iso-surface of averaged Q-Criterion (Q = 2 × $10^5 s^{-2}$) is shown and colored by root mean square (RMS) velocity. Clearly, it can be seen that the boundary layer flow on the suction side appears to be laminar over most of the airfoil surface. Towards the trailing edge, the rollup of two-dimensional turbulent eddies is observed due to boundary layer flow separation and turbulence transition. This progressively becomes three-dimensional when they reach the very aft

location of the trailing edge (≈ 0.9c). On the pressure side the boundary layer separates and turns turbulent just a little further downstream of the step-trip location, where three-dimensional turbulence rotation can be observed clearly. Again, on the suction side the step-trip doesn't show any obvious effect on boundary layer flow and no evident turbulence structures appear. These findings correlate with observations of Winkler et al (2009).

Mean and rms Fields

The mean surface pressure distributions from OpenFOAM LES are compared with the corresponding experimental data (Winkler, 2009) in Figure 5. The LES results from CFX-V11 obtained by Winkler et al (2009, 2008) are plotted in the same figure also. It can be seen that the numerical data obtained in the present study agrees very well with experimental data and the previous LES, and that LES is clearly superior to RANS for this application. The step-trip LES captures the boundary layer separation on the upper surface as occurring at around x/c = 0.8 exactly. Meanwhile, the additional separation occurring on the lower surface, due to the existence of the step-trip at around x/c = 0.25, was clearly observed in both the OpenFOAM LES and Winkler et al CFX LES. However, it was not seen in the experimental measurements. This might be due to insufficient tripping effect of the step-trip that is located just upstream of the separation bubble (Winkler, 2009), but the local pressure peaks occurring due to the boundary layer trips were also predicted properly in OpenFOAM LES, as observed in experiments.

The contours of RMS pressure on the suction side near the trailing edge (x/c = 0.8) and on the pressure side near the step-trip (x/c = 0.25) are shown in Figure 6. Obviously, the pressure fluctuation around the airfoil corresponds to the surface pressure distribution. Large mean pressure variations are observed at the boundary layer separation regimes. In addition, the peak pressure occurring at about 0.8c in Figure 6 (left) corresponds to the local loss of lift seen in Figure 5.

Figure 5 Mean pressure distribution on the airfoil surface

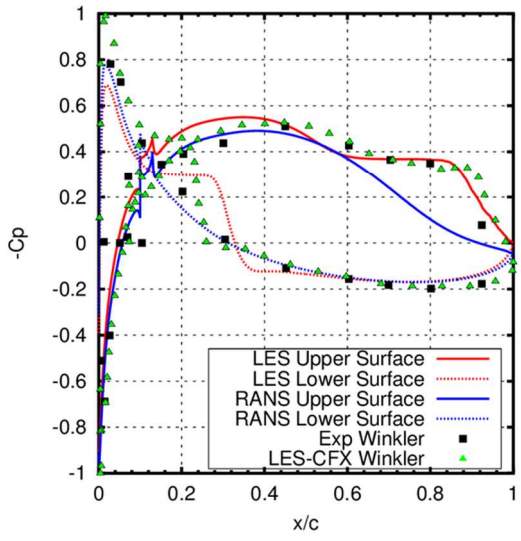

The mean velocity profiles obtained from the step-trip LES in the mid-span plane at various streamwise locations on the suction and the pressure sides are shown in Figure 7. The figures clearly display the boundary layer development and growth as the flow moves downstream. On the suction side, the reverse flow in the boundary layer at x/c = [0.7-0.95] indicates the presence of turbulence separation, as discussed above. On the pressure side, the reversed separated flow is seen at x/c = [0.15-0.3] with a smaller scale. After reattachment of the boundary layer at x/c = 0.45, the mean velocity profile exhibits a typical turbulent boundary layer profile, indicating the turbulence transition has occurred, which agrees very well with above discussion. However, there is no corresponding experimental data for these results.

Figure 6 Contours of rms pressure on the suction side near TE (left) and on the pressure side near step-trip (right)

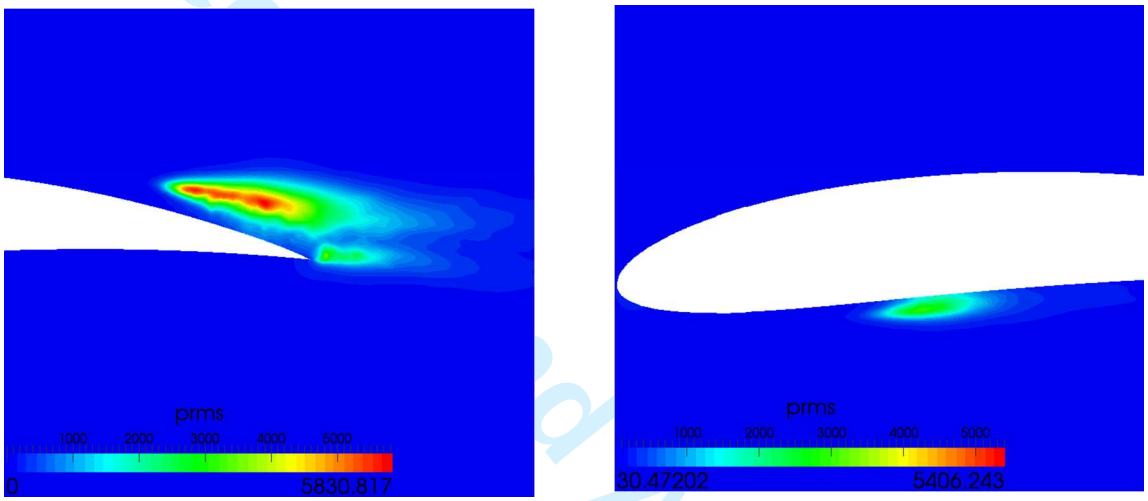

Figure 7 Mean velocity profiles at various streamwise locations on the suction side (left) and the pressure side (right)

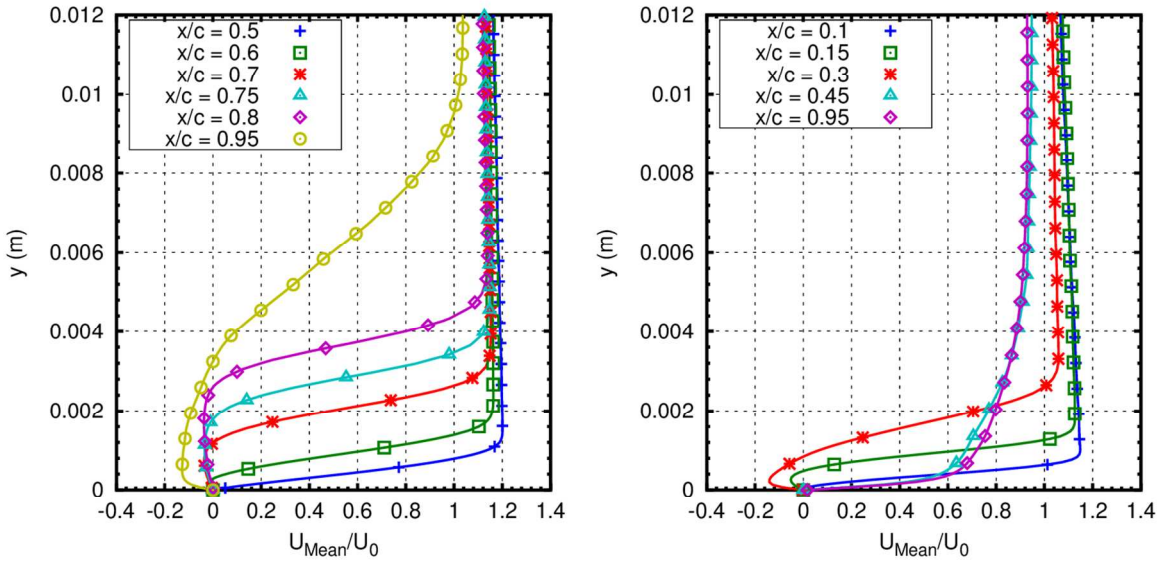

Power Spectral Analysis

In the step-trip LES, the surface pressure signals were collected simultaneously with the flow field averaging process, and then the Sound Pressure Level (SPL)-frequency spectral was obtained by calculating the Fast Fourier Transform (FFT) of

the temporal surface pressure data. In Figure 8, the calculated and measured surface pressure fluctuations, in the form of SPL, are presented together for comparison. The experimental results are for a microphone placed at 1.2 m above the trailing edge and are filtered at Δf = 3.125 Hz for simplicity. The simulation results were not filtered and the results are again for microphones placed at 1.2 m above the trailing edge. It is noted that the SPL is plotted here with respect to a reference pressure of 20 μPa.

It can be seen that the result from the integral acoustic prediction method based on OpenFOAM LES and Curle's acoustic analogy agrees very well with experimental data at low to medium frequency range, while overpredicting the SPL at a high frequency range. A similar observation was reported by Winkler et al (2009). Therefore it is recommended that Curle's analogy is most suitable for noise prediction at low to medium frequency range.

Figure 8 Sound pressure levels from Curle's analogy with reference pressure of 20 μPa

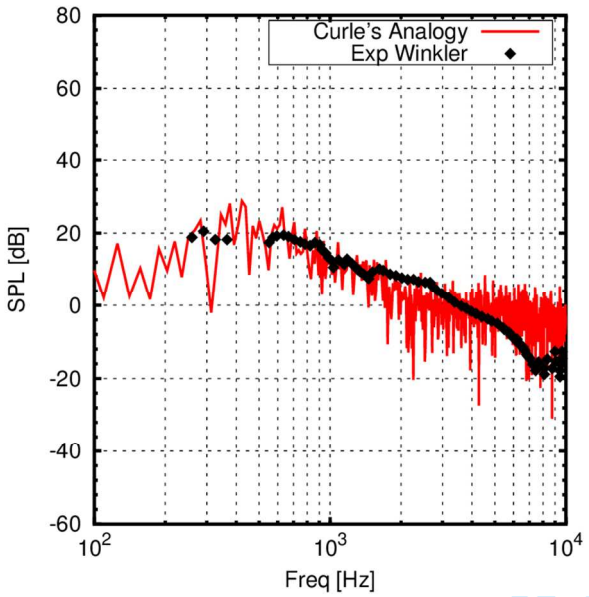

Conclusions

An accurate numerical prediction for the near-field flow around an airfoil/fan-blade and its wake flow development is of outstanding importance for accelerating airfoil self-noise and downstream broadband noise prediction, which has been identified as a significant contributor to modern high-bypass ratio (HBR) engine noise.

In the present study, an integral aeroacoustic prediction method based on Large Eddy Simulation and Curle's acoustic analogy has been thoroughly evaluated in terms of its capability to produce accurate near-field acoustic sources and to predict far-field noise properly. Particularly, the Large Eddy Simulation as implemented in OpenFOAM CFD code has been employed to predict the near-field flow and the boundary layer flow transition, around a NACA6512-63 airfoil with boundary layer tripping at zero angle of attack with Re = 1.9×10^5. The boundary layer tripping used in the experimental

setup to eliminate TS instabilities has been incorporated into the numerical grid as a simplified geometrical step-trip. In order to improve the stability of the numerical simulation and to incorporate the effects of the wind tunnel walls as well, a RANS method with $\kappa - \omega$ Shear Stress Transport equations was used for the whole wind tunnel domain and its result was then interpolated as inlet boundary conditions for the LES domain. Curle's acoustic analogy, which has been recently implemented in OpenFOAM, was used for far-field sound pressure levels prediction and validation.

The numerical results presented in this paper show that near-field unsteady flow features around the NACA6512-63 airfoil, particularly the boundary layer separation near the trailing edge on the suction side and just behind the step-trip on the pressure side, have been correctly captured in OpenFOAM LES calculations. The mean surface pressure distributions for the step-trip setup agree very well with the experimental measurements. Local pressure peaks predicted by the OpenFOAM LES, due to the trip and boundary layer flow separation and transition, were in agreement with the experimental measurements. The RANS interpolated inflow condition was shown good to yield accurate results for the LES airfoil surface pressure distribution, and the lift coefficient predicted by OpenFOAM proved to be as accurate as or better than predictions made by others using CFX previously (Winkler, 2009).

Aeroacoustic prediction using Curle's analogy shows an overall agreement with the experimental data for the airfoil with boundary layer trip. The Sound Pressure Level (SPL)-frequency spectral analysis produces very similar data at low to medium frequency, whereas the experimentally observed levels are slightly over-predicted at a higher frequency range.

It is concluded that the combination of LES with a simple Smagorinsky SGS model and Curle's analogy, as implemented in OpenFOAM CFD code, is capable of predicting the boundary layer flow over the NACA6512-63 airfoil at a moderate Reynolds number $Re = 1.9 \times 10^5$, as well as the airfoil self-noise sources associated with its trailing edge and wake.

References

Li, Y., Wang, X. and Zhang, D. (2013), "Control strategies for aircraft airframe noise reduction," Chinese Journal of Aeronautics, vol. 26, no. 3, pp. 249–260.

Kraposhin, M.V. and Strizhak S.V. (2013) http://www.openfoamworkshop2013.org/file/Tue/Track3-4_SergeiStrizhak_MatveyKraposhin.tar

Smagorinsky, J. (1963), "General Circulation Experiments with the Primitive equations", Monthly Weather Review, vol. 91, no. 3, pp. 99-164.

Winkler, J., Moreau, S and Carolus, T. (2009), "Large-Eddy Simulation and Trailing-Edge Noise Prediction of an Airfoil with Boundary-Layer Tripping", 30th AIAA Aeroacoustics Conference., AIAA-2009-3197, Miami, FL.

Winkler, J. and Moreau, S. (2008), "LES of the Trailing-Edge Flow and Noise of a NACA6512-63 Airfoil at Zero Angle of Attack", Proceedings of the Summer Program 2008, Centre for Turbulence Research., Stanford University/NASA Ames, Stanford, CA, pp. 331–342.

Winkler, J. Moreau, S. and Carolus, T. (2010), “Airfoil Trailing Edge Noise Prediction from Large-Eddy Simulation: Influence of Grid Resolution and Noise Model Formulation”, 16th AIAA/CEAS Aeroacoustics Conference., AIAA Paper 2010-3704, Stockholm, Sweden.

Wang, M., Moreau, S., Laccarino, G. and Roger, M. (2009), “LES Prediction of Wall-Pressure Fluctuations and Noise of a Low-Speed Airfoil”, International Journal of Aeroacoustics, Vol. 8, No. 3, pp. 177– 197.

Addad, Y., Prosser, R., Laurence, D., Moreau, S. and Mendonça, F. (2008), “On the Use of Embedded Meshes in the LES of External Flows, Flow”, Turbulence and Combustion, Vol. 80, No. 3, pp. 393–403.

Moreau, S., Henner, H., Laccarino, G., Wang, M. and Roger, M. (2003), “Analysis of Flow Conditions in Freejet Experiments for Studying Airfoil Self-Noise”, AIAA Journal, Vol. 41, No. 10, pp. 1895–1905.

Ferzinger, J. and Perci, M. (1996), “Computational methods for fluid dynamics”, Springer.

Matouk, R., Degrez, G. and Christophe, J. (2015), “Aerodynamic and Aeroacoustics Study of the Flow Around an Automotive Fan Airfoil”, International Journal of Aeroacoustics, Vol. 14, pp.1049-1070.

Gilling, L. (2009), “Airfoils in Turbulent Inflow”, Aalborg: Department of Civil Engineering, Aalborg University. (DCE Thesis; No. 23).

Vedovoto, J. M., Serfaty, R. and Silveira Neto, A. D. (2015), “Mathematical and Numerical Modeling of Turbulent Flows”, Anais da Academia Brasileira de Ciências, Vol. 87, No. 2, pp. 1195-232.

Lighthill, M.J. (1952), "On sound generated aerodynamically.Part I. General theory", Proceedings of the Royal Society of London , vol. 211, no. 1107 , pp. 564–587.

Curle, N. (1955), "The influence of solid boundaries upon aerodynamic sound," Proceedings of the Royal Society of London, vol. 231, no. 1187, pp. 505–514.

Goldstein, M. E. (1976), Aeroacoustics, McGraw-Hill Book Company, New York, USA.

Nomenclature

Symbols

c	*m*	Chord length	t	s	Time step size
C_p	-	Pressure coefficient	u	*m/s*	Streamwise velocity
f	*Hz*	Frequency	v	*m/s*	Velocity in wall-normal direction
f_s	*Hz*	Sampling frequency			
L_x, L_y, L_z	-	Dimensions of computational cells	x	*m*	Streamwise distance from the airfoil leading edge
M	-	Mach number	x'	*m*	Streamwise distance from the airfoil trailing edge
P	*Pa*	Static pressure			
P_{Ref}	*Pa*	Reference pressure $(= 2 \times 10^{-5})$	y	*m*	Normal distance from the wall surface
Re_c	-	Chord based Reynolds number	y^+	-	Dimensionless wall distance

α	*deg.*	Angle of attack
δ	*m*	Boundary layer thickness
γ	m^2/s	Fluid kinematic viscosity
ρ	kg/m^3	Density
ω	-	Turbulence frequency